PDK4 Augments ER–Mitochondria Contact to Dampen Skeletal Muscle Insulin Signaling During Obesity

Themis Thoudam,[1,2] Chae-Myeong Ha,[1,2] Jaechan Leem,[3] Dipanjan Chanda,[4] Jong-Seok Park,[5] Hyo-Jeong Kim,[6] Jae-Han Jeon,[4,7] Yeon-Kyung Choi,[4,7] Suthat Liangpunsakul,[8,9,10] Yang Hoon Huh,[6] Tae-Hwan Kwon,[1,2] Keun-Gyu Park,[4,7] Robert A. Harris,[9] Kyu-Sang Park,[11] Hyun-Woo Rhee,[12] and In-Kyu Lee[4,7]

Diabetes 2019;68:571–586 | https://doi.org/10.2337/db18-0363

Mitochondria-associated endoplasmic reticulum membrane (MAM) is a structural link between mitochondria and endoplasmic reticulum (ER). MAM regulates Ca^{2+} transport from the ER to mitochondria via an IP3R1-GRP75-VDAC1 complex–dependent mechanism. Excessive MAM formation may cause mitochondrial Ca^{2+} overload and mitochondrial dysfunction. However, the exact implication of MAM formation in metabolic syndromes remains debatable. Here, we demonstrate that PDK4 interacts with and stabilizes the IP3R1-GRP75-VDAC1 complex at the MAM interface. Obesity-induced increase in PDK4 activity augments MAM formation and suppresses insulin signaling. Conversely, PDK4 inhibition dampens MAM formation and improves insulin signaling by preventing MAM-induced mitochondrial Ca^{2+} accumulation, mitochondrial dysfunction, and ER stress. Furthermore, *Pdk4*$^{-/-}$ mice exhibit reduced MAM formation and are protected against diet-induced skeletal muscle insulin resistance. Finally, forced formation and stabilization of MAMs with synthetic ER–mitochondria linker prevented the beneficial effects of PDK4 deficiency on insulin signaling. Overall, our findings demonstrate a critical mediatory role of PDK4 in the development of skeletal muscle insulin resistance via enhancement of MAM formation.

Endoplasmic reticulum (ER) and mitochondria are distinct cellular organelles that are known to physically interact with each other to exchange phospholipids, calcium (Ca^{2+}), and other metabolites to maintain cellular integrity and bioenergetics (1). Contact sites between ER and mitochondria are termed the mitochondria-associated ER membrane (MAM). MAM regulates Ca^{2+} transfer from ER to mitochondria via formation of a macromolecular complex comprising inositol 1,4,5-trisphosphate receptor type 1 (IP3R1), glucose-regulated protein 75 (GRP75), and voltage-dependent anion channel 1 (VDAC1) (2). IP3R1, an ER-resident Ca^{2+} release channel, is physically linked with the mitochondrial outer membrane protein VDAC1 via molecular chaperone GRP75. Several reports have shown that MAM plays a critical role in obesity-induced hepatic insulin resistance (IR) (3–5), although it is controversial whether the formation of MAMs prevents (3,5)

[1]Department of Biomedical Science, The Graduate School, Kyungpook National University, Daegu, Republic of Korea
[2]BK21 Plus KNU Biomedical Convergence Program, Department of Biomedical Science, Kyungpook National University, Daegu, Republic of Korea
[3]Department of Immunology, School of Medicine, Catholic University of Daegu, Daegu, Republic of Korea
[4]Leading-Edge Research Center for Drug Discovery and Development for Diabetes and Metabolic Disease, Kyungpook National University Hospital, Daegu, Republic of Korea
[5]Department of Chemistry, Ulsan National Institute of Science and Technology, Ulsan, Republic of Korea
[6]Electron Microscopy Research Center, Korea Basic Science Institute, Ochang, Chungbuk, Republic of Korea
[7]Department of Internal Medicine, School of Medicine, Kyungpook National University, Kyungpook National University Hospital, Daegu, Republic of Korea
[8]Division of Gastroenterology and Hepatology, Department of Medicine, Indiana University School of Medicine, Indianapolis, IN
[9]Department of Biochemistry and Molecular Biology, Indiana University School of Medicine, Indianapolis, IN
[10]Richard L. Roudebush VA Medical Center, Indianapolis, IN
[11]Department of Physiology, Institute of Lifestyle Medicine, Yonsei University Wonju College of Medicine, Gangwon-Do, Republic of Korea
[12]Department of Chemistry, Seoul National University, Seoul, Republic of Korea

Corresponding author: In-Kyu Lee, leei@knu.ac.kr

Received 29 March 2018 and accepted 20 November 2018

This article contains Supplementary Data online at http://diabetes.diabetesjournals.org/lookup/suppl/doi:10.2337/db18-0363/-/DC1.

T.T., C.-M.H., J.L., and D.C. contributed equally to this work.

or promotes (4) IR. Given that skeletal muscle is a major site for regulating whole-body glucose homeostasis (6), these findings prompted us to investigate whether MAMs prevent or promote IR in skeletal muscle.

Although the molecular mechanisms underlying skeletal muscle IR are not fully understood, mitochondrial dysfunction has been implicated to play a key role in the development of this pathological condition (7). Accumulating evidence suggests that ER stress contributes to the development of IR (8). Recent studies have shown that deregulation in Ca^{2+} transfer from ER to mitochondria via MAM can cause ER stress and mitochondrial dysfunction (4,5). For example, disruption of Ca^{2+} transfer between the two organelles by pharmacological and genetic inhibition of cyclophilin D led to ER stress and mitochondrial dysfunction in mouse hepatocytes and liver, resulting in the development of IR (5). Furthermore, it was recently reported by the same group that disruption of sarcoplasmic reticulum (SR)/ER–mitochondria interaction in both skeletal muscle of obese mice and palmitate-treated myotubes is associated with IR, whereas enhancement of MAM prevents IR (9). However, the findings we report here have led us to the opposite conclusion.

Pyruvate dehydrogenase kinases (PDKs) are mitochondrial enzymes that suppress the conversion of pyruvate to acetyl CoA via inhibitory phosphorylation of the pyruvate dehydrogenase complex (PDC) (10). To date, four isoenzymes of PDK (PDK1, 2, 3, and 4) have been identified in mammals and are expressed in a tissue-specific manner (11). Among them, PDK4 is predominantly expressed in skeletal muscle and heart. Previous studies have shown that PDK4 expression is dramatically increased in skeletal muscle of insulin-resistant patients and rodents (12,13). High-fat diet (HFD)–challenged *Pdk4*$^{-/-}$ mice exhibit improved glucose tolerance and insulin sensitivity (13,14), suggesting that PDK4 may be a potential therapeutic target against IR and its associated comorbidities (10). Although the beneficial effects of PDK4 deficiency on IR are believed to be associated with PDC activation and subsequent increase of glucose oxidation, the exact molecular mechanism remains unclear. Recently, we have reported that PDK4 inhibition is closely associated with improvement of mitochondrial function in several tissues during metabolic stress (15,16). In addition, PDK4 was found in a proteomic study to be present in the MAM fraction of skeletal muscle (17). Based on these findings, we speculated that PDK4 might play a role in the physical and/or functional communication between SR/ER and mitochondria in skeletal muscle.

RESEARCH DESIGN AND METHODS

Animal Models

Male 8-week-old wild-type (WT) and *Pdk4*$^{-/-}$ C57Bl/6J mice (13) originating from The Jackson Laboratory (Bar Harbor, ME) were fed a control diet (CD) or 60% HFD (D12492; Research Diets, Inc., New Brunswick, NJ) and housed in a pathogen-free and temperature-controlled room (12:12 h light/dark cycle) for 16 weeks. Muscle tissues were harvested from these mice after 16 weeks on the diets and from male *ob/ob* mice under fed conditions (Central Lab. Animal, Inc., Seoul, South Korea) when they were 12 weeks old. For insulin infusion, mice fasted for 16 h were injected with insulin (10 mU/g body weight) intraperitoneally for 10 min. All experiments were performed in accordance with and approved by the Institutional Animal Care and Use Committee of Kyungpook National University.

Cell Lines

The C2C12 cell line was purchased from ATCC (Manassas, VA). WT and VXY/PDK4-flag–expressing C2C12 myoblasts were cultured in DMEM high-glucose media (#SH30243.01; Hyclone, Queensland, Australia) supplemented with 10% FBS (#SH30084.03; Hyclone) and 1× Antibiotic-Antimycotic (#15240-062; Gibco, Auckland, New Zealand). Cells were differentiated into myotubes with DMEM containing 2% horse serum (Gibco) for 5 days.

Primary Skeletal Muscle Cells

Primary myotube and myoblast culture was performed with gastrocnemius muscle harvested from 8-week-old WT or *Pdk4*$^{-/-}$ mice as described previously (18).

siRNA, Plasmids, and Adenovirus Constructs

siRNAs targeting PDK4 (#1406883), GRP75 (#1370988), IP3R1 (#1374717), PDHE1α (#1406708), and Foxo1 (#1359213) and control siRNA (#SN-1003) were purchased from Bioneer (Daejeon, South Korea). PDK4 kinase dead (ΔPDK4-flag) plasmid construct was designed by deleting the nucleic acid sequence that encodes the aspartate and tryptophan DW (Asp^{394}-Trp^{395}) motif as previously reported (19). D1ER and 4mitD3 plasmids were provided by K.-S.P. (Yonsei University, Gangwon-Do, South Korea). Mitochondria-targeted blue fluorescence protein (mito-BFP), mitochondria-targeted GFP (mito-GFP), ER-targeted Sec61B-GFP, and a similar synthetic ER–mitochondria linker (Linker-RH) plasmid used in previous reports (4,20) were provided by H.-W.R. (Seoul National University, Seoul, South Korea). Linker-RH carries mitochondria outer membrane–targeted A kinase anchor protein 1 (AKAP1), Linker (20), red fluorescent protein (RFP) mCherry, ER integral membrane protein phosphatidylinositide phosphatase Sac1, and hemagglutinin (HA) encoding sequences to obtain a 15- to 20-nm space between the ER and mitochondria outer membrane. The vector backbone of all of the constructs is pcDNA3. PDK4 adenovirus was provided by Dr. Y.-B. Kim (Harvard Medical School). pcDNA and mock adenovirus served as control for transient transfection and adenovirus transduction, respectively.

Transient Transfection and Adenovirus Transduction

For myoblast, siRNA (100 nmol/L) or plasmid DNA was transfected using RNAi Max reagent (13778150; Thermo

Fisher Scientific) or Lipofectamine 2000 (11668019; Thermo Fisher Scientific), respectively, and cultured for 48 h. For myotubes, siRNA was transfected on the 3rd day of differentiation and incubated for 2 days before any treatment. Adenovirus Linker-RH was transduced in C2C12 myotubes or primary myotubes for 48 h.

Experimental Treatments

C2C12 myotubes were treated with BSA (A7030; Sigma-Aldrich, St. Louis, MO) or BSA-conjugated 0.4 mmol/L palmitate (P9767; Sigma-Aldrich) with or without 4 mmol/L dichloroacetate (DCA) (Sigma-Aldrich) for 16 h, thapsigargin (Tg) (Sigma-T9033) 0.25 μmol/L or DMSO (D2650; Sigma-Aldrich) for various times, or JNK inhibitor SP600125 (Enzo Life Sciences) 20 μmol/L for 6 h. For insulin stimulation, the cells were incubated in serum-free medium containing 100 nmol/L insulin (I6634; Sigma-Aldrich) for 10 min.

In Situ Proximity Ligation Assay

In situ proximity ligation assays (PLAs) in C2C12 cells were performed as described previously (3). For isolated single myofibers, myofibers were washed with PBS, fixed with 4% paraformaldehyde, and permeabilized with 0.2% Triton-X in 0.1 mol/L glycine/PBS, followed by blocking and overnight incubation with primary antibodies at 4°C. Myofibers were washed, probed with secondary antibodies conjugated with oligonucleotide, ligated, and amplified using an in situ PLA kit (DUO92101, Duolink; Sigma-Aldrich). Images were captured using an Olympus FluoView FV1000 confocal microscope or Olympus 1 × 81 fluorescence microscope (Olympus Imaging, Center Valley, PA). In situ PLA blobs were counted using MetaMorph software (Molecular Devices, San Jose, CA). Detailed antibody information is given in Supplementary Table 1.

Immunofluorescence Analysis

C2C12 myoblasts were grown on coverslips, transfected with plasmid DNA, incubated for 24 h, washed with PBS, fixed with 4% paraformaldehyde, permeabilized, and mounted with VECTASHIELD Mounting Medium (H1200). Images were captured using an Olympus FluoView FV1000 confocal microscope. Pearson coefficient colocalization was analyzed by ImageJ software with Fiji plugin (National Institutes of Health, Bethesda, MD).

Subcellular Fractionation

Subcellular fractionation of C2C12 myotubes and gastrocnemius muscle (nonstarved mice) was performed as previously described (21,22).

Coimmunoprecipitation and Immunoblotting

Cells or tissues were lysed in lysis buffer (50 mmol/L Tris, 150 mmol/L Nacl, 1% Triton X-100, 1 mmol/L EDTA, and 10% glycerol) with protease (04693132001; Roche) and phosphatase inhibitors (P0044; Sigma-Aldrich). A total of 500 μg protein lysate was incubated with GRP75 antibody and Protein A/G PLUS-Agarose beads (2003; Santa Cruz Biotechnology) or anti-FLAG M2 Magnetic Beads (M8823; Sigma-Aldrich) overnight at 4°C. The solution was washed with lysis buffer, and protein bound to the beads was eluted with sample buffer and boiled.

For immunoblotting, cells or tissues were lysed in radioimmunoprecipitation assay lysis buffer with protease and phosphatase inhibitors. Protein samples were resolved by SDS-PAGE and transferred to polyvinylidene difluoride membranes. Detailed antibody information is given in Supplementary Table 1. PDK3 and 4 anti-serum was obtained from R.A.H. (Indiana University, Indianapolis, IN). Intensity of immunoblot bands was quantified using ImageJ software.

Subcellular Ca^{2+} Measurement

C2C12 cells were cultured on coverslips with Fura-2 AM (Life Technologies), washed with Ca^{2+}-free Krebs-Ringer bicarbonate buffer, and transferred to a perfusion chamber on an inverted microscope IX-70 (Olympus). The samples were alternately excited at 340 and 380 nm by a monochromatic light source LAMDA DG-4 (Sutter Instrument Company, Novato, CA). Fluorescence images were captured at 510 nm with an intensified CCD camera (Roper Scientific, Trenton, NJ). The two excitation wavelength (F340/F380) fluorescence intensity ratio was estimated by using MetaFluor 6.1 software (Molecular Devices). ER and mitochondrial Ca^{2+} were measured with fluorescence resonance energy transfer–based protein probe D1ER and 4mitD3, respectively. Transfected cells were excited at 440 nm and YFP (540 nm) and CFP (490 nm) emission wavelength monitored by the Nikon Ti-E inverted microscope equipped with a Cascade 512B (EMCCD) camera (Roper Scientific). The ratiometric recording of emitted fluorescence from YFP (540 nm) and CFP (490 nm) was created by MetaMorph software (Molecular Devices).

Transmission Electron Microscopy

Tissues and cells were fixed with 2.5% glutaraldehyde, stained with 1% osmium tetroxide, washed with PBS, dehydrated in ethanol and propylene oxide, embedded in epon 812, and polymerized. Sections were counterstained with uranyl acetate and lead citrate and visualized with a Bio-HVEM system (JEM-1400 Plus at 120 kV and JEM-1000 BEF at 1,000 kV; JEOL Ltd., Tokyo, Japan). ImageJ software was used for measuring the mitochondrial perimeter and surface area of MAM (distance between ER/SR and mitochondria within 30 nm).

Mitochondrial Reactive Oxygen Species Measurement

Reactive oxygen species (ROS) were measured using ROS-sensitive MitoTracker red CM-H2XRos (M7513 Molecular Probes/Life Technologies) and ROS-insensitive MitoTracker green FM (M7514; Molecular Probes/Life Technologies) as previously described (23). The ratio between

red and green fluorescence was quantified and analyzed using ImageJ software.

Mitochondrial Membrane Potential Measurement

Mitochondrial membrane potential (MMP) was assessed using JC-1 dye (Molecular Probes) by flow cytometer (FACSCalibur; BD Biosciences). JC-1 red/green ratio was analyzed using CellQuest Pro 4.0 software.

ATP Measurement

ATP was measured using an ATPlite luminescence assay (6016943; PerkinElmer) by following the manufacturer's protocol and normalized with protein concentration.

Oxygen Consumption Rate

Oxygen consumption rate was measured using an XF-24 flux analyzer as previously described (15).

mtDNA Quantification

mtDNA and genomic DNA (gDNA) were isolated with DNeasy Kit (69504; Qiagen) and quantified by real-time PCR as previously described (24).

Statistical Analysis

Statistical significance was determined by the unpaired Student *t* test when two groups were compared. One- or two-way ANOVA was used for comparisons among multiple groups. Values are presented as the mean ± SD of the indicated number of independent samples. P values <0.05 were considered statistically significant.

RESULTS

PDK4 Interacts With IP3R1-GRP75-VDAC1 Complex at the MAM Interface

We first validated the presence of the IP3R1-GRP75-VDAC1 complex at the MAM. Subcellular fractions isolated from C2C12 myotubes (Supplementary Fig. 1*A*) or mouse gastrocnemius muscle (Fig. 1*A*) demonstrated the occurrence of these proteins in the MAM fraction. We then evaluated the interactions between these proteins at the MAM interface via in situ PLA. We observed that IP3R1, GRP75, and VDAC1 interact with each other in C2C12 myoblasts (Supplementary Fig. 1*B*). These interactions were reconfirmed by coimmunoprecipitation (co-IP) in both C2C12 myotubes (Supplementary Fig. 1*C*) and mouse gastrocnemius muscle (Fig. 1*C*). Additionally, ryanodine receptor 1 (RyR1), a Ca^{2+} channel that also serves as a conduit for Ca^{2+} release from the SR/ER, was detected in the MAM fraction (Fig. 1*A*), but we did not observe any interactions between RyR1 and GRP75 or VDAC1 (Fig. 1*C* and Supplementary Fig. 1*B* and *C*). We then examined the effects of silencing IP3R1 or GRP75 on the interactions among IP3R1, GRP75, and VDAC1. Knockdown of IP3R1 (Supplementary Fig. 1*D*) decreased the interaction between GRP75 and VDAC1 as well as its interactions with GRP75 or VDAC1 (Supplementary Fig. 1*E*). Likewise, knockdown of GRP75 (Supplementary Fig. 1*F*) reduced the interaction between IP3R1 and VDAC1 as well as its interactions with IP3R1 or VDAC1 (Supplementary Fig. 1*G*). Taken together, these findings suggest that IP3R1, GRP75, and VDAC1 form a multiprotein complex at the MAM interface in skeletal muscle.

We investigated whether PDK4 is present at the MAM interface in skeletal muscle and C2C12 myotubes. PDK4 was detected abundantly in the mitochondrial fraction but not in the SR/ER fraction (Fig. 1*A* and Supplementary Fig. 1*A*). Interestingly, among the four PDK isoenzymes, only PDK4 was detected in the MAM fraction (Fig. 1*A*). To look for a potential role for PDK4 in MAM, we determined whether PDK4 interacts with the other MAM proteins by in situ PLA with C2C12 myoblasts stably expressing PDK4-flag or VXY control. PDK4 clearly interacts with IP3R1, GRP75, and VDAC1 but not RyR1 (Fig. 1*B*). This observation was further validated by co-IP, in which GRP75 immunoprecipitated PDK4 along with VDAC1 and IP3R1 (Fig. 1*C*). Similarly, co-IP with anti-flag antibody confirmed that PDK4 physically interacts with GRP75, IP3R1, and VDAC1 (Fig. 1*D*).

We then investigated the subcellular site of the interaction between PDK4 and IP3R1, GRP75, or VDAC1 by overlaying the in situ PLA blobs with mito-GFP. We observed that most of the interactions are in the vicinity of the mitochondrial outer surface (Supplementary Fig. 1*H*). In addition, we transfected the PDK4-flag stable cells with Sec61b-GFP and mito-BFP to track ER and mitochondria, respectively (Fig. 1*E*). The in situ PLA blobs of PDK4-flag/IP3R1 as well as IP3R1-VDAC1 were localized at the ER–mitochondria interface, as visualized by confocal microscope (Fig. 1*F*). Taken together, these results indicated that PDK4 interacts with the IP3R1-GRP75-VDAC1 complex at the MAM interface.

PDK4 Kinase Activity Is Crucial for MAM Formation

PDK4 is a serine/threonine kinase. We examined whether its kinase activity is required for interacting with the components of the IP3R1 channeling complex. To this end, we performed in situ PLA (Fig. 2*A* and *B*) and co-IP (Fig. 2*C*–*E*) in PDK4-flag–overexpressing C2C12 cells in the absence or presence of DCA, a known synthetic inhibitor of PDKs. DCA treatment suppressed the interaction of PDK4 with IP3R1, GRP75, or VDAC1 (Fig. 2*A* and *C*–*E*). In addition, enhanced IP3R1-GRP75-VDAC1 interactions induced by PDK4-flag overexpression were markedly reduced by DCA treatment (Fig. 2*B*). To be more specific, we constructed a kinase activity dead PDK4 (ΔPDK4-flag) mutant. Overexpression of ΔPDK4-flag failed to induce PDHE1α (a component of PDC) phosphorylation at the serine 293 and 300 residues (Supplementary Fig. 2*A*), confirming the loss of its kinase activity. Unlike PDK4-flag, ΔPDK4-flag overexpression failed to induce IP3R1-GRP75-VDAC1 interactions (Fig. 2*F*). Moreover, we did not observe any interaction between PDHE1α and IP3R1 or VDAC1 (interaction between PDHE1α and

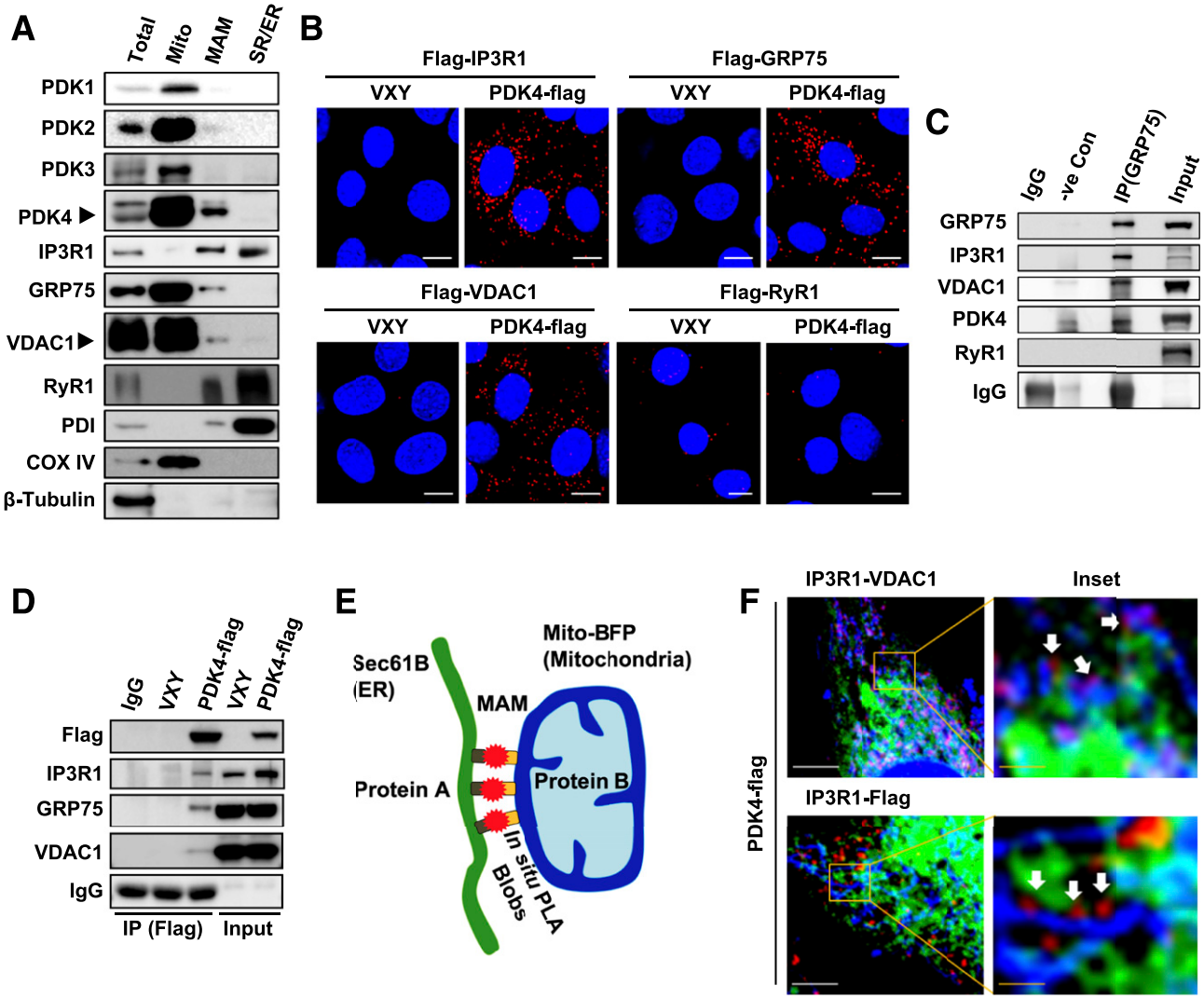

Figure 1—PDK4 resides and interacts with the IP3R1-GRP75-VDAC1 complex at the MAM interface. *A*: Immunoblot analysis of subcellular fractions isolated from gastrocnemius muscle in mice. Markers for MAM and SR/ER (protein disulfide isomerase [PDI]), mitochondria (cytochrome c oxidase [COX IV]), nucleus (proliferating cell nuclear antigen [PCNA]), and cytosol (β-tubulin). *B*: In situ PLA in VXY control and PDK4-flag C2C12 myoblasts (scale bars, 10 μm). *C*: Coimmunoprecipitation (IP) analysis in gastrocnemius muscle homogenate in mice. *D*: IP analysis in VXY- (control) and PDK4-flag–expressing C2C12 myotubes. *E*: Schematic illustration depicting detection of protein–protein interaction by in situ PLA at the MAM interface using ER-targeted Sec61B-GFP and mitochondria-targeted mito-BFP. *F*: Confocal microscope imaging of in situ PLA blobs at the MAM interface (indicated by white arrows) in PDK4-flag–expressing C2C12 myoblasts (scale bars, 5 μm; inset, yellow scale bars, 1 μm). -ve Con, negative control.

PDK2 in the absence and presence of siPDHE1α was used as negative and positive controls, respectively) (Supplementary Fig. 2*B*). Additionally, siRNA-mediated knockdown of PDHE1α did not affect the IP3R1-GRP75-VDAC1 interactions in the basal or PDK4-overexpressed condition (Supplementary Fig. 2*C*–*E*). Taken together, these results suggest that the PDK4 promotes IP3R1-GRP75-VDAC1 complex formation independent of PDC activity.

Obesity Augments MAM Formation in Skeletal Muscle

Next, we examined the role of PDK4 in MAM formation in the context of obesity-induced skeletal muscle IR. To understand the role of MAM formation in obesity, mice were sacrificed in the fed state to rule out the independent effects of fasting on MAM formation. As previously reported (13), we observed a robust increase in the level of PDK4 protein, but not of PDK1, 2, or 3, in skeletal muscle of HFD-fed and genetically obese *ob/ob* mice compared with CD-fed and lean mice, respectively (Fig. 3*A* and *B*). Increased plasma free fatty acid levels, especially palmitate, are associated with obesity and lipotoxicity and play a critical role in the development of obesity-induced IR (25). Similarly, palmitate-treated C2C12 myotubes show elevated levels of PDK4 protein but not of other isoenzymes (Supplementary Fig. 3*A* and *B*). Interestingly,

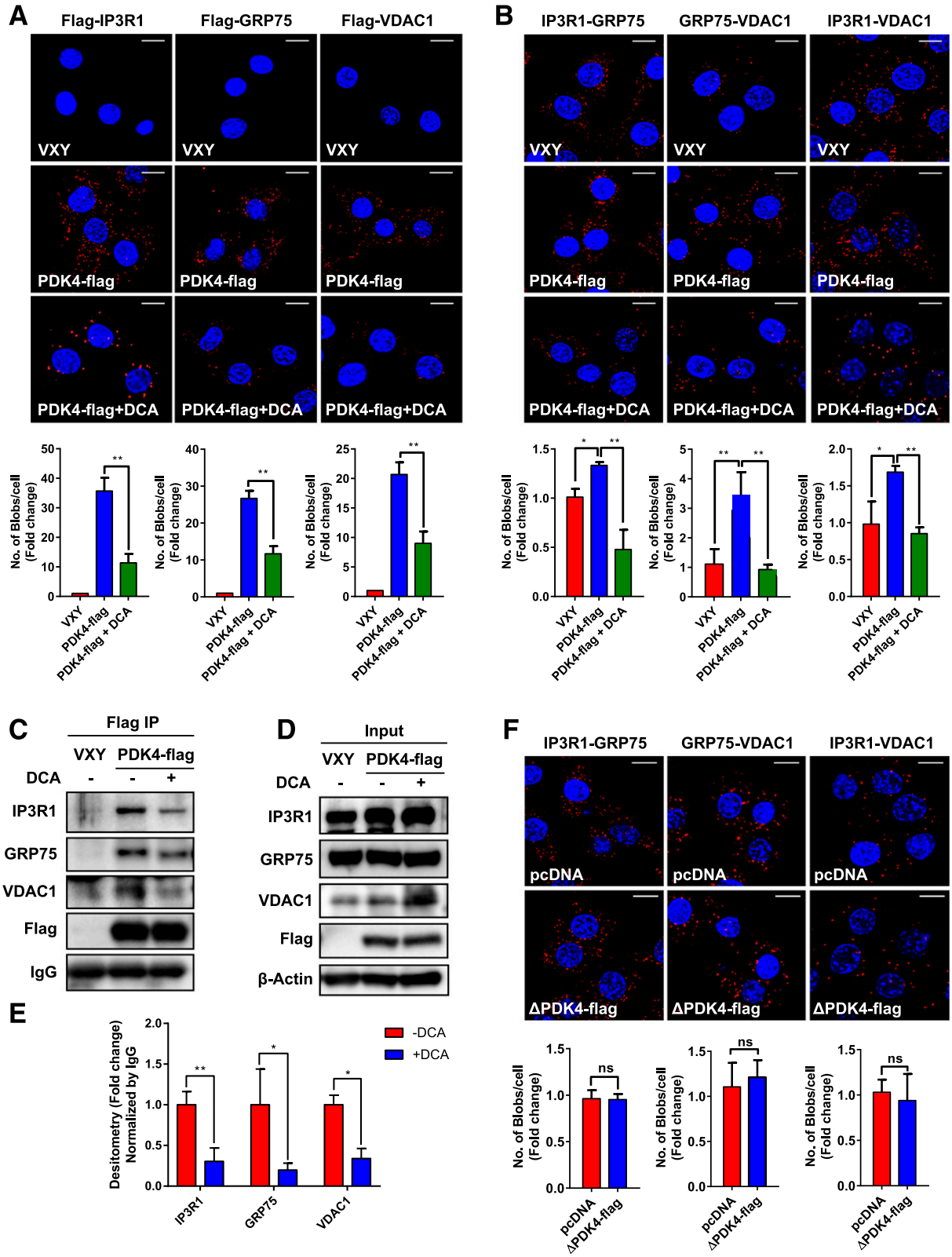

Figure 2—Inhibition of PDK4 kinase activity suppresses MAM formation. *A* and *B*: In situ PLA in VXY- and PDK4-flag–expressing C2C12 myoblasts ± 4 mmol/L DCA for 6 h (respective panels are quantified below). Scale bars, 20 μm; mean ± SD of $n = 3$ of >30 cells/experiment (*$P < 0.05$; **$P < 0.01$; one-way ANOVA). *C*: Coimmunoprecipitation (IP) analysis in VXY- and PDK4-flag–expressing C2C12 myotubes ± 4 mmol/L DCA for 6 h. *D*: Input controls of *C*. *E*: Quantification of *C* (mean ± SD of $n = 3$) (*$P < 0.05$, **$P < 0.01$, Student *t* test). *F*: In situ PLA in C2C12 myoblasts that were transfected with either pcDNA or ΔPDK4-flag (respective panels are quantified below). Scale bars, 20 μm; mean ± SD of $n = 3$ of >30 cells/experiment. ns, not significant.

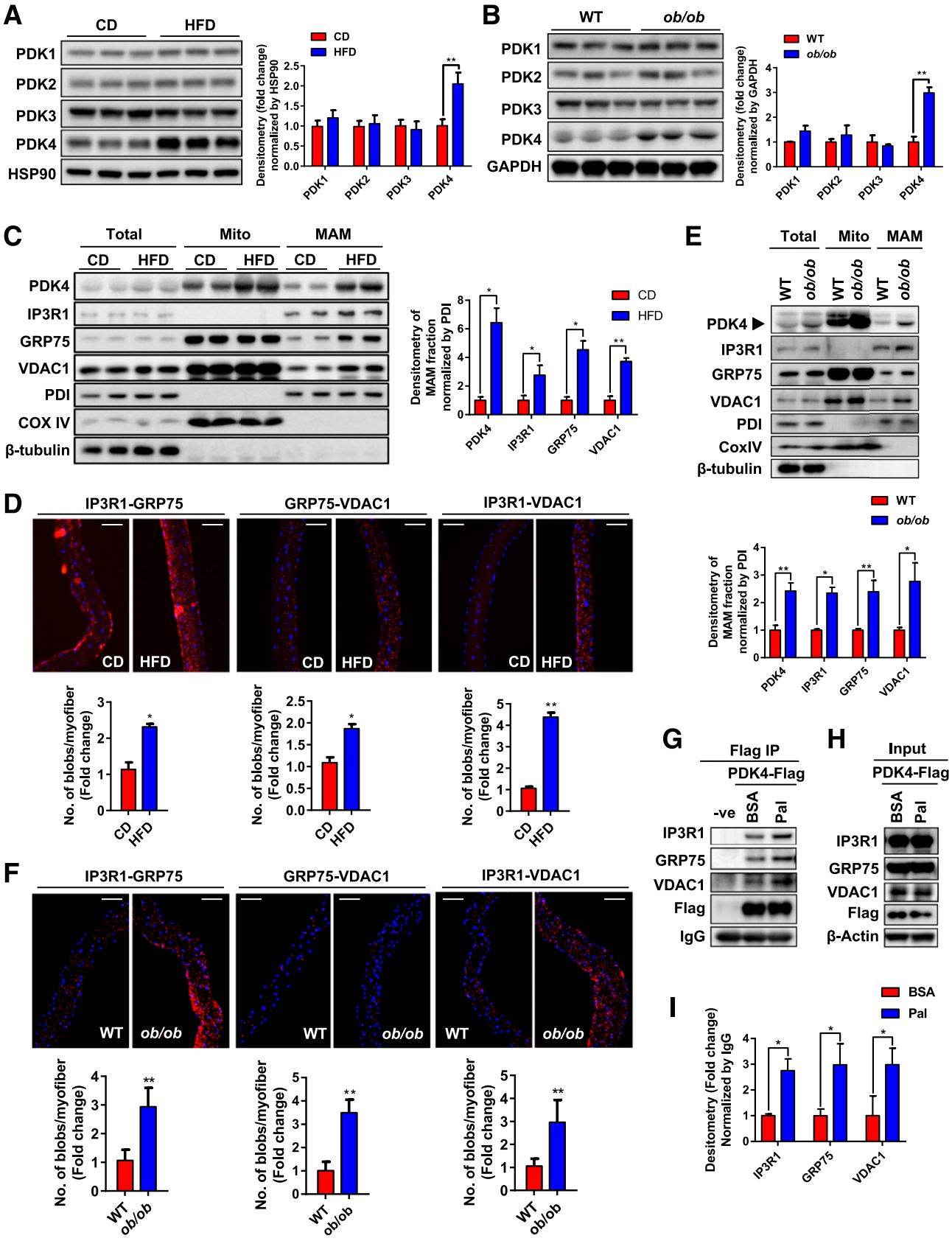

Figure 3—Obesity enhances MAM formation in skeletal muscle. *A*: Immunoblot analysis of gastrocnemius muscle isolated from CD- and HFD-fed mice (left) and quantification (mean ± SD of n = 6/group; $^{**}P < 0.01$, Student t test). *B*: Immunoblot analysis of gastrocnemius muscle isolated from WT and *ob/ob* mice (left) and quantification (mean ± SD of n = 3/group; $^{**}P < 0.01$, Student t test) (right). *C*: Representative immunoblot analysis of subcellular fractions isolated from gastrocnemius muscle of CD- or HFD-fed mice (left) and

we observed a significant enrichment of PDK4 along with other known MAM proteins, IP3R1, GRP75, and VDAC1, in the MAM fraction of HFD-fed mice (Fig. 3*C*) or upon palmitate treatment (Supplementary Fig. 3*C*). Moreover, IP3R1-GRP75-VDAC1 interactions were significantly increased in the myofibers isolated from HFD-fed mice compared with CD-fed mice, as visualized by in situ PLA (Fig. 3*D*). Additionally, the MAM fraction isolated from *ob/ob* mice has increased PDK4, IP3R1, GRP75, and VDAC1 protein levels compared with lean mice (Fig. 3*E*). In situ PLA in myofibers isolated from *ob/ob* mice also showed enhanced IP3R-GRP75-VDAC1 interactions (Fig. 3*F*). Altogether, these findings indicate enhanced MAM formation in skeletal muscle during obesity.

To investigate the effect of palmitate on the integrity of the IP3R1 channeling complex, we monitored IP3R1-VDAC1 interaction by in situ PLA. Palmitate treatment increases IP3R1-VDAC1 interaction along with a concomitant increase in PDK4 protein level (Supplementary Fig. 3*D*, *E*, and *H*). Additionally, we also evaluated whether glucose has any synergistic effect on palmitate-induced IP3R1-VDAC1 interaction. However, we did not observe any significant effect of glucose at either low or high concentration on palmitate-induced dose-dependent increase in IP3R1-VDAC1 interaction (Supplementary Fig. 3*F* and *G*). Several transcription factors including PPARα, PPARγ, PGC1α, and FoxO1 have been reported to regulate PDK4 expression (26). Among these, dephosphorylation and activation of FoxO1 are closely associated with PDK4 induction in vitro and in vivo (Supplementary Fig. 3*H* and *I*). Palmitate-induced upregulation of PDK4 was reversed by FoxO1 siRNA, but not of PDK2 (Supplementary Fig. 3*J*). Furthermore, co-IP assay demonstrated that the interaction of PDK4 with IP3R1, GRP75, or VDAC1 was significantly increased upon palmitate treatment (Fig. 3*G–I*). Taken together, these results indicate that PDK4 enrichment in the MAM during obesity is associated with enhanced mitochondria–ER/SR interactions in the skeletal muscle of obese mice.

PDK4 Ablation Hinders MAM Formation in Skeletal Muscle of Mice With Diet-Induced Obesity

Next, we examined whether genetic ablation of PDK4 could suppress MAM formation in mice with diet-induced obesity. To evaluate this, we isolated subcellular fractions from gastrocnemius muscle of WT and *Pdk4*$^{-/-}$ mice fed with a CD or HFD. We observed that the expression levels of MAM-resident proteins in total homogenates from skeletal muscle of *Pdk4*$^{-/-}$ mice were comparable to those in WT mice. In addition, HFD feeding did not affect their expression levels in WT or *Pdk4*$^{-/-}$ mice (Supplementary Fig. 4*A* and *B*). However, HFD-induced enrichment of these proteins in the MAM fraction from skeletal muscle of WT mice was reduced in *Pdk4*$^{-/-}$ mice (Fig. 4*A* and *B*). Moreover, in situ PLA of myofibers isolated from gastrocnemius muscle of HFD-fed *Pdk4*$^{-/-}$ mice exhibited a reduction in IP3R1-VDAC1-GRP75 interactions compared with HFD-fed WT mice (Fig. 4*C*), indicating a reduction in MAM formation. Similarly, palmitate-induced increase in IP3R1-GRP75 or VDAC1 interactions and enrichment of IP3R1 in crude mitochondrial fraction (MAM containing mitochondrial extract) were significantly decreased upon PDK4 knockdown (Supplementary Fig. 4*C–E*). Furthermore, transmission electron microscopy (TEM) analysis of gastrocnemius muscle showed significantly increased intermyofibrillar (IMF) MAM (SR/ER and mitochondria contacts within a 30-nm distance) surface area in HFD-fed WT mice compared with controls. *Pdk4*$^{-/-}$ mice significantly reversed this effect (Fig. 4*D* and *E*). In addition, the distance between SR/ER and mitochondria in MAM was taken into account considering the irregular distance (0–30 nm) observed in TEM images. A distance (>15 nm) between SR/ER and mitochondria, which is considered to be loose MAM, is required for accommodating IP3R1-VDAC1-GRP75 complex formation and to transfer Ca^{2+} efficiently, whereas a <15 nm (tight MAM) distance is considered unsuitable for Ca^{2+} transfer (27). Interestingly, we observed an increase in loose MAM and reduction in tight MAM percentage in total MAM surface area in HFD-fed WT mice compared with controls or HFD-fed *Pdk4*$^{-/-}$ mice (Fig. 4*F*). However, MAM was not observed in subsarcolemmal mitochondria (Supplementary Fig. 4*F*). Similarly, populations of ER-associated mitochondria and MAM surface area were significantly increased in palmitate-treated WT myoblasts, and this effect was reduced in *Pdk4*$^{-/-}$ myoblasts (Supplementary Fig. 4*G–I*). Next, we asked whether deficiency of PDK4 has any effect on basal mitochondrial dynamics that might negatively affect the structural integrity of MAM. To this end, we evaluated the expression level of proteins that are involved in mitochondrial fusion and fission machinery. PDK4 deficiency had no effect on the expression level of fusion proteins Mfn1, Mfn2, and OPA1, or fission proteins Fis1 and Drp1, and the regulatory phosphorylation sites (S616 and S637)

quantification of MAM fractions (mean ± SD of $n = 3$/group; $^*P < 0.05$; $^{**}P < 0.01$, Student *t* test) (right). *D*: In situ PLA in isolated myofibers from CD- and HFD-fed mice (respective panels are quantified below). Scale bars, 100 μm; mean ± SD of ~10–15 myofibers/sample ($^*P < 0.05$, $^{**}P < 0.01$, Student *t* test). *E*: Immunoblot analysis of subcellular fractions isolated from gastrocnemius muscle of WT and *ob/ob* mice (top) and quantification of MAM fractions (representative of gastrocnemius skeletal muscle pooled from $n = 6$ mice/group; mean ± SD of $n = 3$) ($^*P < 0.05$, $^{**}P < 0.01$, Student *t* test) (bottom). *F*: In situ PLA in isolated myofibers from WT and *ob/ob* mice (respective panels are quantified below). Scale bars, 100 μm; mean ± SD of ~10–20 myofibers/sample ($^{**}P < 0.01$, Student *t* test). *G*: Coimmunoprecipitation (IP) analysis in PDK4-flag–overexpressing C2C12 myotubes treated with 0.4 mmol/L palmitate (Pal)/BSA for 16 h. *H*: Input control of *G*. *I*: Quantification of *G* (mean ± SD of $n = 3$; $^*P < 0.05$, Student *t* test). -ve, negative control.

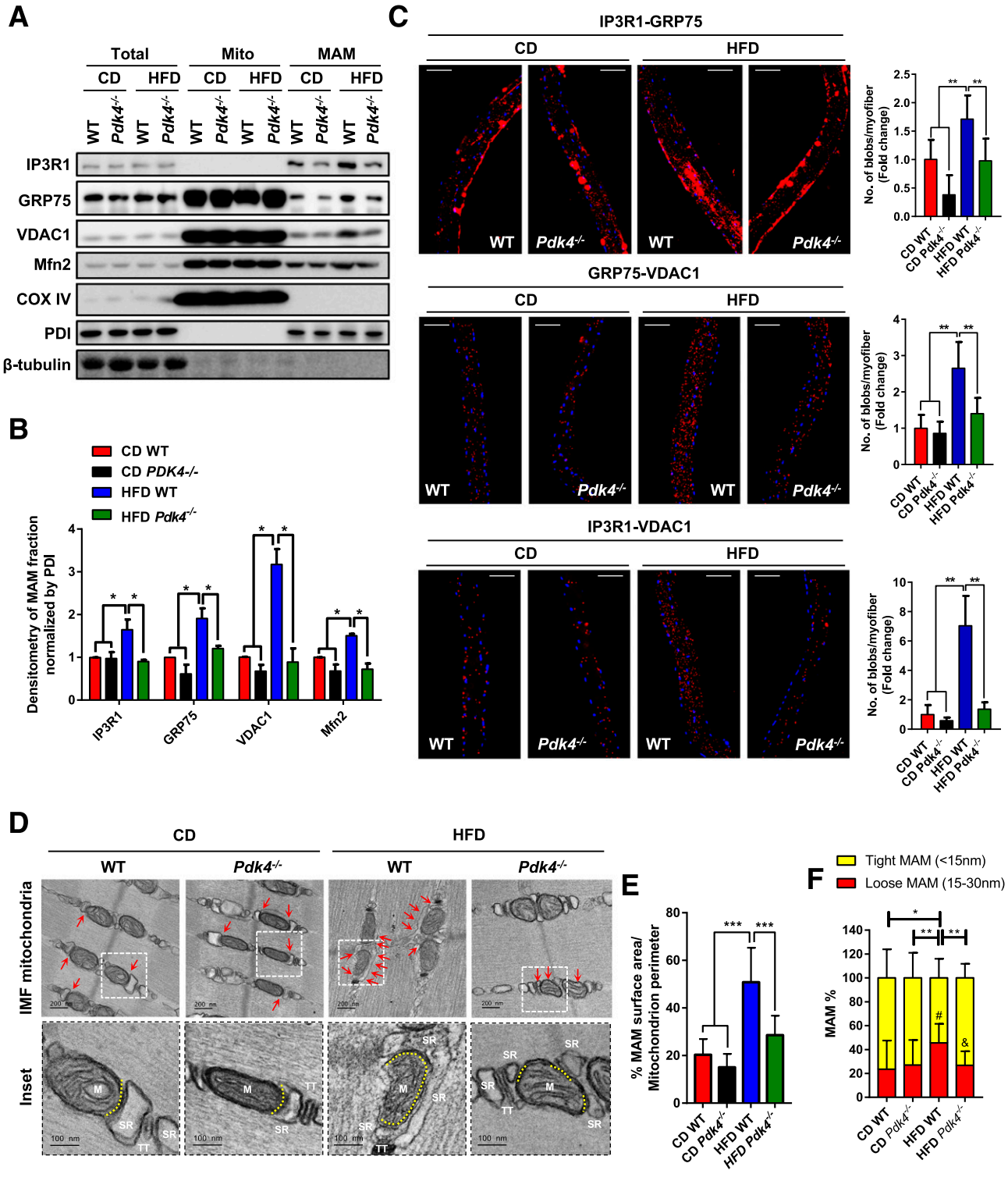

Figure 4—Genetic ablation of PDK4 reduced MAM formation in skeletal muscle of mice with diet-induced obesity. *A*: Immunoblot analysis of subcellular fractions isolated from CD- or HFD-fed WT and *Pdk4*$^{-/-}$ mice. *B*: Quantification of proteins in MAM fraction of *A* (gastrocnemius muscle pooled from $n = 6$ mice/group, and two independent experiments were performed) (*$P < 0.05$, one-way ANOVA). *C*: In situ PLA in isolated myofibers from CD- or HFD-fed WT and *Pdk4*$^{-/-}$ mice (scale bars, 100 μm) (left) and quantification of in situ PLA blobs (mean ± SD of ~10–20 myofibers/sample) (**$P < 0.01$, one-way ANOVA) (right). *D*: Representative TEM images showing the association of SR/ER and IMF in gastrocnemius muscle isolated from CD- or HFD-fed WT and *Pdk4*$^{-/-}$ mice (red arrows indicate the SR–mitochondria contact sites) (scale bars, 200 nm). Inset: yellow dotted line indicating the surface area of MAM (M, mitochondria; TT, T-tubule) (inset scale bars, 100 nm). *E*: Percentage of MAM surface area per mitochondrion perimeter in each microscopic field ($n = 20$/group; mean ± SD; ***$P < 0.001$, one-way ANOVA). *F*: Percentage of tight MAM (<15 nm) and loose MAM (15–30 nm) in total MAM surface area ($n = 28$–41/group; mean ± SD; *$P <$ 0.05, **$P < 0.01$, #$P < 0.05$ control vs. WT HFD; &$P < 0.05$ WT HFD vs. *Pdk4*$^{-/-}$ HFD, one-way ANOVA).

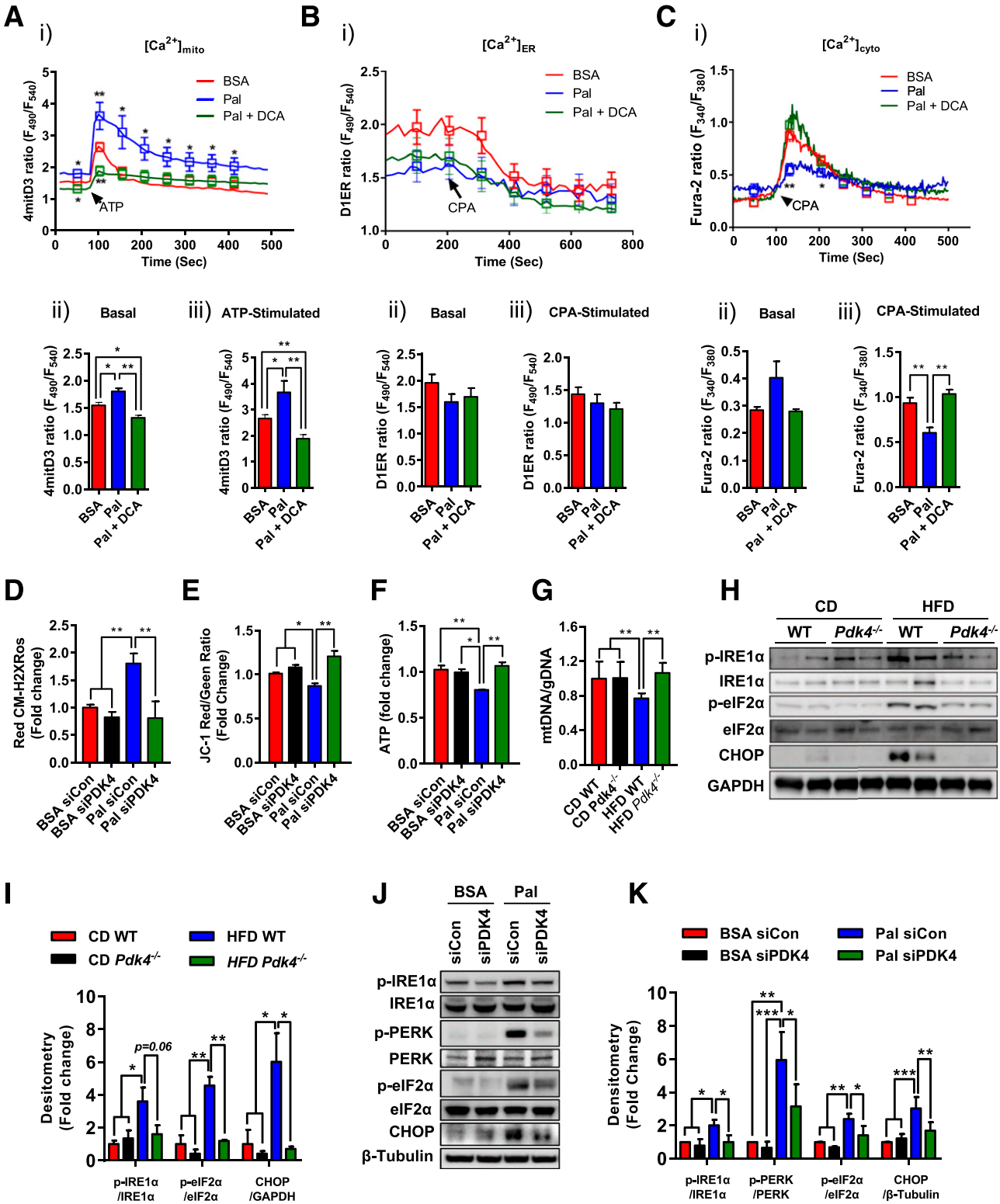

Figure 5—PDK4 inhibition attenuates MAM-mediated Ca^{2+} transfer from ER to mitochondria, mitochondrial dysfunction, and ER stress. *A*: Mitochondrial Ca^{2+} flux was measured using 4mitD3 probe (*Ai*). Basal $[Ca^{2+}]_{mito}$ (*Aii*) and $[Ca^{2+}]_{mito}$ after stimulation with 500 nmol/L ATP (*Aiii*) in C2C12 myoblast treated with 50 μmol/L palmitate (Pal)/BSA and ± 4 mmol/L DCA for 16 h (n = 9–12/group; mean ± SD; $^*P < 0.05$, $^{**}P < 0.01$, one-way ANOVA). *B*: ER lumen Ca^{2+} was measured using D1ER (*Bi*). Basal $[Ca^{2+}]_{ER}$ (*Bii*) and $[Ca^{2+}]_{ER}$ after stimulation with 1 μmol/L CPA (*Biii*) in C2C12 myoblast treated with 50 μmol/L Pal/BSA and ± 4 mmol/L DCA for 16 h (n = 9–12/group; mean ± SD). *C*: Cytosolic Ca^{2+} measurement using Fura-2 dye (*Ci*). Basal $[Ca^{2+}]_{cyto}$ (*Cii*) and $[Ca^{2+}]_{cyto}$ after stimulation with 1 μmol/L CPA (*Ciii*) in C2C12 myoblast treated with 50 μmol/L Pal/BSA and ± 4 mmol/L DCA for 16 h (n = 9–12/group; mean ± SD; $^{**}P < 0.01$, one-way ANOVA). *D*: Evaluation of mitochondrial ROS generation after 16-h incubation with 0.4 mmol/L Pal/BSA in control siRNA (siCon)/siPDK4-transfected C2C12 myotubes using CM-H2XRos normalized by MitoTracker green FM (n = 3; mean ± SD; $^{**}P < 0.01$, one-way ANOVA). *E*: MMP in

(Supplementary Fig. 4*A*, *B*, *J*, and *K*). Moreover, we did not observe any significant difference in total, IMF, and subsarcolemmal mitochondrial perimeter between WT and *Pdk4*$^{-/-}$ skeletal muscle (Supplementary Fig. 4*L*). In addition, basal mitochondria oxygen consumption rate was similar between WT and *Pdk4*$^{-/-}$ myotubes (Supplementary Fig. 4*M* and *N*). Altogether, these results suggest that PDK4 deficiency reduces MAM formation in skeletal muscle under metabolic stress.

PDK4 Inhibition Attenuates Ca^{2+} Transfer From ER to Mitochondria, Mitochondrial Dysfunction, and ER Stress

MAM plays a key role in regulating Ca^{2+} transfer from ER to mitochondria via formation of the IP3R1 channeling complex (2). Previous studies have demonstrated that metabolic stress enhances Ca^{2+} transfer from ER to mitochondria, resulting in mitochondrial Ca^{2+} overload (4,28). Therefore, to determine the role of PDK4 in palmitate-induced Ca^{2+} transfer between the two organelles, we measured mitochondrial Ca^{2+} levels in C2C12 myoblasts using a mitochondria-specific Ca^{2+} probe, 4mitD3 (29). As expected, the basal $[Ca^{2+}]_{mito}$ levels were significantly higher in palmitate-treated cells compared with vehicle. However, cotreatment of DCA lowered basal $[Ca^{2+}]_{mito}$ level compared with palmitate treatment (Fig. 5*A*i and ii). In addition, we detected a higher peak of $[Ca^{2+}]_{mito}$ following stimulation of IP3R-mediated ER Ca^{2+} release by ATP (30) upon palmitate treatment. These effects of palmitate were attenuated in the presence of DCA (Fig. 5*A*i and iii). We next measured $[Ca^{2+}]_{ER}$ levels using D1ER, an ER-specific Ca^{2+} probe (31), after stimulating with vehicle, palmitate, or palmitate/DCA. Both the basal and cyclopiazonic acid (CPA) (SR/ER Ca^{2+}-ATPase inhibitor)–induced ER Ca^{2+} depletion rates were similar in all groups, suggesting that PDK4 inhibition does not affect the ER Ca^{2+} store or release machinery (Fig. 5*B*i–iii). Additionally, we also monitored $[Ca^{2+}]_{cyto}$ using Fura-2, a cytosolic Ca^{2+} indicator, but failed to notice any significant difference among the groups (Fig. 5*C*i and ii). However, draining out of $[Ca^{2+}]_{ER}$ by CPA in palmitate-treated cells released less Ca^{2+} to cytosol, thereby suggesting that a major portion of the ER Ca^{2+} goes to mitochondria due to enhanced MAM formation. This effect was reversed upon PDK4 inhibition by DCA (Fig. 5*C*i and iii). Taken together, these results indicate that suppression of MAM formation by PDK4 inhibition decreases palmitate-induced Ca^{2+} transfer from ER to mitochondria.

Enhanced Ca^{2+} transfer from ER to mitochondria via MAM can cause ER stress and mitochondrial dysfunction (4,32). Thus, we investigated whether disruption of MAM could attenuate ER stress and mitochondrial dysfunction in skeletal muscle in the context of obesity. Palmitate-induced mitochondrial ROS generation was significantly suppressed by silencing PDK4 as well as components of the IP3R1 channeling complex, such as GRP75 or IP3R1 (Fig. 5*D* and Supplementary Fig. 5*A*). As previously reported (33), palmitate treatment resulted in a reduction of MMP. These effects were reversed upon knockdown of PDK4 (Fig. 5*E*). Furthermore, palmitate-induced decrease in ATP production was also reversed by silencing PDK4 or other MAM components, GRP75 or IP3R1 (Fig. 5*F* and Supplementary Fig. 5*B*). Mitochondrial density and activity play a crucial role in skeletal muscle function (34). Interestingly, deficiency of PDK4 prevented the depletion of mtDNA copy number in HFD-fed mice (Fig. 5*G*). However, the mitochondrial OXPHOS complex protein level was similar among the groups (Supplementary Fig. 5*C* and *D*).

Next, we asked whether disruption of MAM could attenuate obesity-induced ER stress. Both HFD and palmitate-induced ER stress as observed by increased IRE1a, eIF2a phosphorylation, and CHOP expression were markedly suppressed in *Pdk4*$^{-/-}$ mice (Fig. 5*H* and *I*) or upon PDK4 knockdown (Fig. 5*J* and *K*). Similar results were obtained upon IP3R1 or GRP75 silencing (Supplementary Fig. 5*E* and *F*), suggesting that disruption of MAM formation attenuates palmitate-induced ER stress.

ER stress inducer Tg, an SR/ER Ca^{2+}-ATPase inhibitor, enhances ER Ca^{2+} depletion and induces mitochondria Ca^{2+}-dependent apoptosis (35). Tg-induced ER stress and IP3R1-VDAC1 interaction were reversed upon PDK4 knockdown (Supplementary Fig. 5*G*–*L*). We also observed that disruption of the IP3R1 channeling complex by GRP75 knockdown suppressed Tg-induced CHOP expression, whereas enhancement of IP3R1 channeling by PDK4 overexpression further amplified Tg-induced CHOP expression. However, this effect of PDK4 overexpression was suppressed by knockdown of GRP75 (Supplementary Fig. 5*M*). Taken together, these results suggest that PDK4 inhibition suppresses induction of ER stress and mitochondrial dysfunction via downregulation of MAM formation (Supplementary Fig. 5*N*).

siCon/siPDK4-transfected C2C12 myotubes using JC-1 dye by FACS. Graph indicates the JC-1 Red and Green ratio ($n = 3$; mean ± SD; *$P <$ 0.05, **$P < 0.01$, one-way ANOVA). *F*: Cellular ATP level was measured in siCon/siPDK4-transfected C2C12 myotubes by ATPlite luminescence assay ($n = 3$; mean ± SD; *$P < 0.05$, **$P < 0.01$, one-way ANOVA). *G*: Quantitative RT-PCR measurement of mtDNA (mitochondrial ND1) normalized by gDNA (nuclear Pecam1) in gastrocnemius muscle of CD- or HFD-fed WT and *Pdk4*$^{-/-}$ mice ($n = 5$/group; mean ± SD; **$P < 0.01$, one-way ANOVA). *H*: Representative immunoblot analysis of ER stress markers in gastrocnemius muscle tissue of CD- or HFD-fed WT and *Pdk4*$^{-/-}$ mice. *I*: Quantification of *H* (mean ± SD of $n = 4$ to 5/group; *$P < 0.05$, **$P < 0.01$, one-way ANOVA). *J*: Representative immunoblot analysis of ER stress markers in siCon/siPDK4-transfected C2C12 myotubes. *K*: Quantification of *J* (mean ± SD of $n = 4$; *$P <$ 0.05, **$P < 0.01$, ***$P < 0.001$, one-way ANOVA). p-, phosphorylated; Sec, seconds.

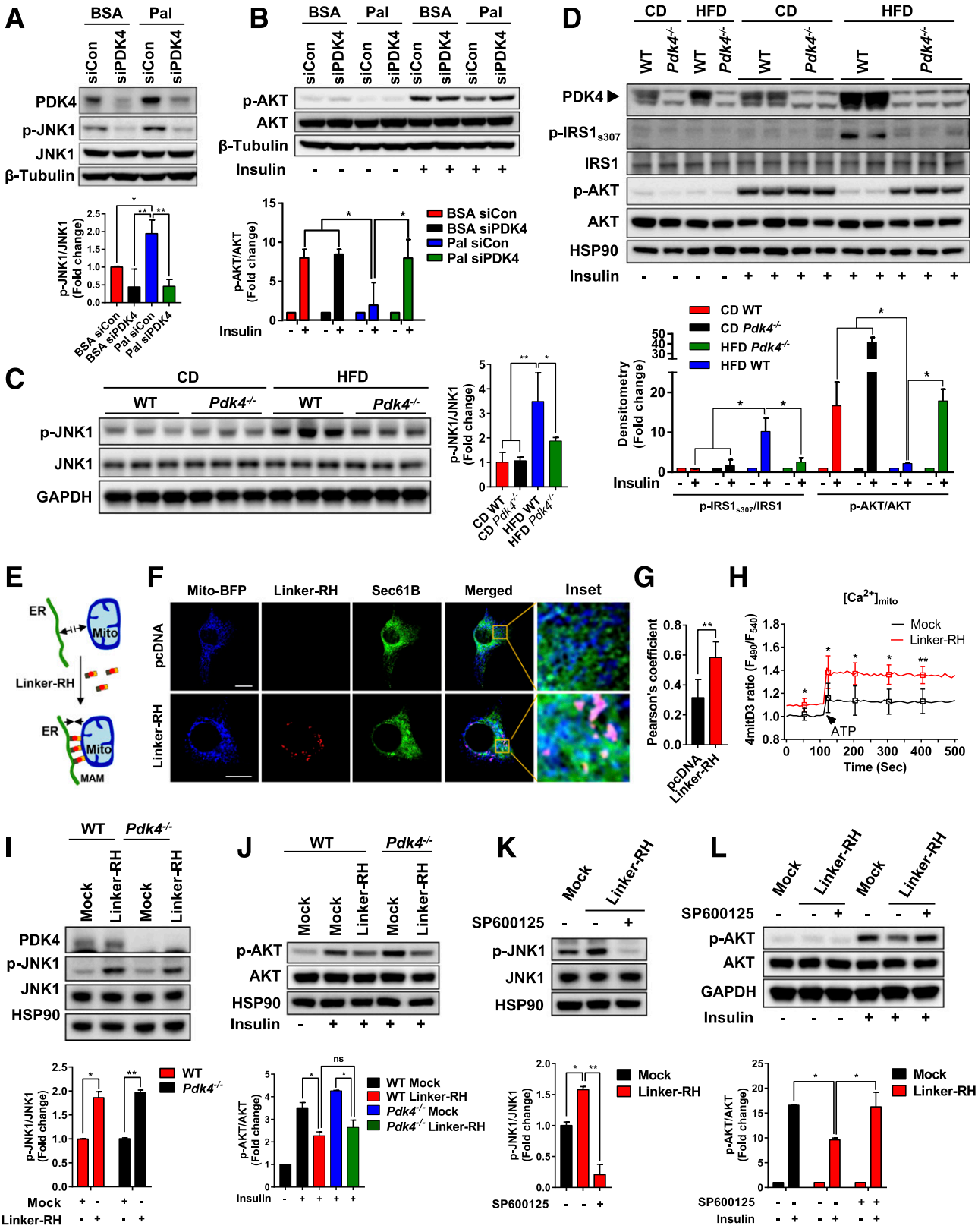

Figure 6—PDK4 deficiency attenuates palmitate (Pal)–induced skeletal muscle IR via downregulation of MAM. *A*: Immunoblot analysis in control siRNA (siCon)/siPDK4-transfected C2C12 myotubes (top) and quantification (mean ± SD of $n = 3$; $^*P < 0.05$, $^{**}P < 0.01$, one-way ANOVA) (bottom). *B*: Immunoblot analysis in siCon/siPDK4-transfected C2C12 myotubes following 100 nmol/L insulin treatment for 10 min (top) and quantification (mean ± SD of $n = 3$; $^*P < 0.05$, one-way ANOVA) (bottom). *C*: Immunoblot analysis in gastrocnemius muscle homogenate isolated from CD- or HFD-fed WT or *Pdk4*$^{-/-}$ mice (left) and quantification (mean ± SD of $n = 3$/group; $^*P < 0.05$, $^{**}P < 0.01$, one-way ANOVA) (right). *D*: Immunoblot analysis of insulin action in CD- or HFD-fed WT or *Pdk4*$^{-/-}$ mice (top) and quantification (mean ± SD of $n = 3$ to 4/group; $^*P < 0.05$, one-way ANOVA) (bottom). *E*: Graphical representation of synthetic ER–mitochondria linker: linker-RFP HA

PDK4 Ablation Attenuates Obesity-Induced Skeletal Muscle IR via Downregulation of MAM

ER stress–mediated JNK activation plays a critical role in the pathogenesis of IR by phosphorylating insulin receptor substrate 1 at serine 307, which subsequently impairs an insulin-induced AKT signaling pathway in skeletal muscle (36). Thus, we examined the effect of JNK1 activation on MAM formation. We observed that palmitate-induced JNK1 activation and inhibition of insulin-induced AKT phosphorylation were reversed upon knockdown of PDK4 (Fig. 6*A* and *B*), suggesting PDK4 knockdown attenuates palmitate-induced impairment of insulin signaling. Similarly, knockdown of IP3R1 or GRP75 reduced JNK1 activation in palmitate-treated cells (Supplementary Fig. 6*A* and *C*) and restored insulin-stimulated AKT signaling (Supplementary Fig. 6*B* and *D*). Furthermore, HFD-induced JNK1 activation and inhibition of insulin-induced AKT phosphorylation were markedly reversed in gastrocnemius muscle of *Pdk4*$^{-/-}$ mice. In addition, inhibitory phosphorylation of IRS-1 at serine 307 was significantly decreased in gastrocnemius muscle of HFD-fed *Pdk4*$^{-/-}$ mice compared with WT mice (Fig. 6*C* and *D*). Taken together, these results suggest that genetic ablation of PDK4 dampens MAM formation and obesity-induced skeletal muscle IR via suppression of JNK activation.

Finally, to demonstrate the causal relationship between PDK4 and MAM in IR, we asked whether the enhancement of MAM formation could reverse the effects of PDK4 deficiency on palmitate-induced IR. To this end, we used a synthetic ER–mitochondria linker (Linker-RH) to artificially enhance SR/ER–mitochondria interaction (Fig. 6*E*). The Linker-RH expression significantly increased ER–mitochondria interaction and mitochondrial (both basal and stimulated) Ca^{2+} levels (Fig. 6*F–H*). Linker-RH expression induced JNK1 phosphorylation and attenuated insulin-induced AKT phosphorylation in C2C12 myotubes (Supplementary Fig. 6*E* and *F*), suggesting that an increase in MAM formation is sufficient to trigger IR. Furthermore, we examined whether PDK4 deficiency could reverse the effect of the Linker-RH. Surprisingly, deficiency of PDK4 failed to suppress linker-mediated JNK1 activation and insulin-induced AKT phosphorylation (Fig. 6*I* and *J* and Supplementary Fig. 6*G* and *H*), indicating that MAM formation occurs downstream of PDK4 signaling. Interestingly, JNK inhibitor SP600125 treatment significantly reversed the inhibitory effect of Linker-RH expression on AKT phosphorylation (Fig. 6*K* and *L*), thereby indicating that the linker-mediated induction of IR is dependent on JNK activation. Altogether, we conclude that PDK4 inhibition improves insulin signaling via suppression of MAM formation in skeletal muscle.

DISCUSSION

ER and mitochondria cross talk via MAM is believed to play a critical role in the maintenance of cellular homeostasis. Dysregulation of MAM is implicated in several human diseases (37). The MAM-resident multiprotein complex IP3R1-GRP75-VDAC1 regulates Ca^{2+} transport from the ER to the mitochondria. Previous reports have demonstrated the importance of this multiprotein complex and its association with hepatic IR (3,4). However, with skeletal muscle being a major tissue affected during IR, the role of MAM and its regulation in the context of the IR remained unclear. Here, we have found that a PDK4 subpopulation resides at MAM and directly interacts with the IP3R1-GRP75-VDAC1 complex to regulate obesity-induced MAM formation, thereby implicating a key regulatory role of PDK4 in the pathogenesis of skeletal muscle IR (Fig. 7). RyR1 is another type of SR/ER Ca^{2+} release channel that is highly expressed in skeletal muscle (38). Because we observed the presence of RyR1 in the MAM, we speculated that RyR1 might be an interacting partner of GRP75 and VDAC1 to regulate Ca^{2+} transfer from SR/ER to mitochondria at the MAM interface. However, we did not observe such interactions. It was previously shown that the cross talk between IP3R1 and RyR1 contributes to Ca^{2+} spark in skeletal muscle (39,40). Thus, we speculate that the presence of RyR1 in the MAM might amplify Ca^{2+} release from SR/ER in response to IP3R1-mediated local Ca^{2+} spark. Further study is required to explore the potential cross talk between the IP3R1 channeling complex and RyR1 in the MAM.

Pharmacological inhibition of PDK activity with DCA and experiments with a PDK4 kinase-deleted mutant demonstrated that kinase activity of PDK4 plays an essential role in the regulation of MAM formation. Interestingly, we have found that knockdown of PDHE1α, the substrate for PDK4 in the PDC (10), did not affect the integrity of the IP3R1-GRP75-VDAC1 complex, suggesting that regulation of MAM formation by PDK4 is

(Linker-RH)–mediated MAM induction. *F*: Targeting of Linker-RH at MAM interface was examined in C2C12 myoblast using mito-BFP (mitochondria) and Sec61B (ER) by confocal microscopy (scale bars, 20 μm). *G*: Pearson coefficient for colocalization between mito-BFP (mitochondria) and Sec61B (ER) in pcDNA- or Linker-RH–transfected C2C12 myoblast (mean ± SD of $n = 8$; $^{**}P < 0.01$, Student *t* test). *H*: Basal and stimulated (with 500 nmol/L ATP) mitochondrial Ca^{2+} flux was measured in mock or Linker-RH–transduced C2C12 myoblast using 4mitD3 probe (n = 9–12/group; mean ± SD; $^{*}P < 0.05$, $^{**}P < 0.01$, Student *t* test). *I*: Immunoblot analysis after mock or Linker-RH transduction in WT or *Pdk4*$^{-/-}$ primary myotubes (top) and quantification (mean ± SD of $n = 3$/group; $^{*}P < 0.05$, $^{**}P < 0.01$, Student *t* test) (bottom). *J*: AKT activation, following 10 min of 100 nmol/L insulin stimulation, was evaluated in mock or Linker-RH–transduced WT or *Pdk4*$^{-/-}$ primary myotubes (top). Bottom: quantification (mean ± SD of $n = 3$/group; $^{*}P < 0.05$, Student *t* test). *K*: JNK phosphorylation was evaluated after mock or Linker-RH transduction in DMSO or 20 μmol/L SP600125 treated for 6 h in WT primary myotubes (top). Bottom: quantification (mean ± SD of $n = 3$; $^{*}P < 0.05$, $^{**}P < 0.01$, Student *t* test). *L*: Insulin-induced AKT activation was evaluated in mock or Linker-RH–transduced WT primary myotubes treated with DMSO or 20 μmol/L SP600125 for 6 h (top). Bottom: quantification (mean ± SD of $n = 3$; $^{*}P < 0.05$, Student *t* test). Sec, seconds.

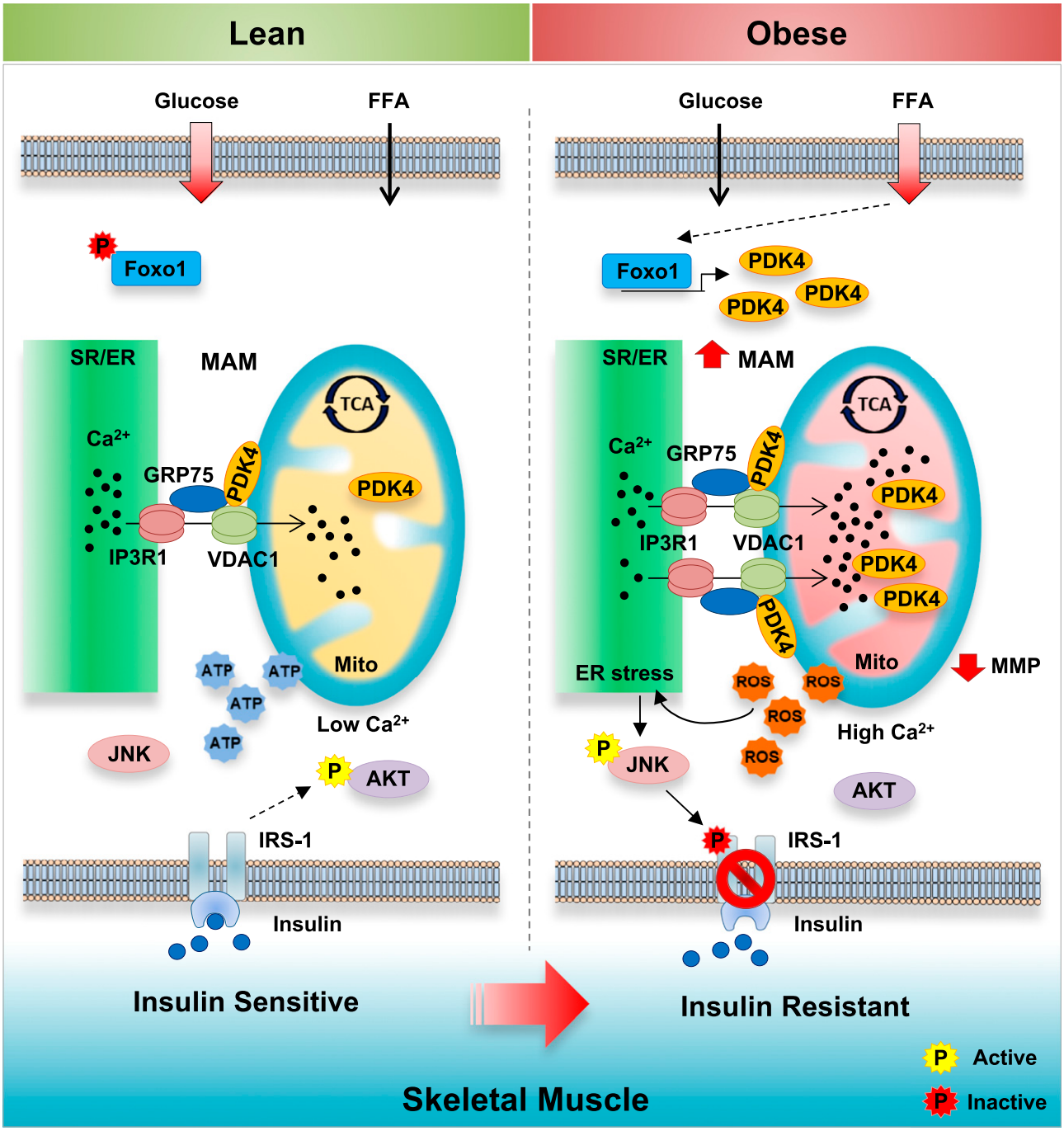

Figure 7—A graphical representation demonstrating the role of PDK4 in obesity-induced MAM formation and skeletal muscle IR. In skeletal muscle, PDK4 interacts with and stabilizes the IP3R1-GRP75-VDAC1 complex at the MAM interface. In physiological conditions, PDK4 is expressed at low levels, and moderate Ca^{2+} transfer from ER to mitochondria via the IP3R1-GRP75-VDAC1 complex formation stimulates mitochondrial ATP production. However, obesity- or free fatty acid (FFA)–induced overexpression of PDK4 via Foxo1 activation augments MAM formation and promotes mitochondrial Ca^{2+} accumulation, mitochondrial dysfunction, and ER stress. Subsequently, ER stress-mediated JNK activation leads to inhibition of the insulin signaling pathway.

independent of PDC. Although target substrates for PDK4 other than PDHE1α have not been firmly established, we speculate that PDK4 might be able to phosphorylate one of these interacting partners in MAM, a hypothesis that warrants future investigation. Furthermore, it can be hypothesized that there are two subpopulations of PDK4: one regulating the PDC complex in mitochondrial matrix to suppress pyruvate oxidation, whereas the second subpopulation is involved in MAM formation and Ca^{2+} transport to mitochondria, thereby contributing toward fatty acid metabolism (via the tricarboxylic acid cycle). Mitochondrial Ca^{2+} is a key molecule that drives the tricarboxylic acid

cycle and ATP synthesis by stimulating isocitrate dehydrogenase, α-keto glutarate dehydrogenase, and ATP synthase (41). We showed that palmitate induces IP3R1-VDAC1 interaction in a time-dependent manner. As described in previous reports (28,42), it is very likely that in the early phase, MAM formation might be beneficial to boost fatty acid oxidation and ATP production, but sustained MAM formation induced by palmitate leads to a constant rise in mitochondrial Ca^{2+} level, which subsequently leads to increased ROS generation and mitochondrial dysfunction. In this context, previous studies demonstrated opposing effects of short-term (43) versus prolonged exposure (44) of palmitate on fatty acid oxidation. Mitochondrial ROS is known to trigger ER stress (32). Therefore, our findings suggest that PDK4 inhibition prevents fatty acid–induced mitochondrial Ca^{2+} accumulation and ROS generation, leading to improvement of mitochondrial dysfunction and ER stress via suppression of MAM formation.

The role of MAM in obesity-induced IR has been investigated in hepatic tissue, but it is still controversial due to contradictory lines of evidence (3–5). In this study, we have observed that MAM is markedly increased in skeletal muscle of both diet- and genetically induced obesity. Our findings are consistent with a previous study showing that excessive ER–mitochondrial coupling contributes to the development of hepatic IR (4). Recently, and contradictory to our current findings, Tubbs et al. (9) reported that MAM formation in skeletal muscle is disrupted as a consequence of diet-induced obesity in mice. We suspect that the discrepancy is due to a major difference in diets used in the studies. The high-fat, high-sucrose diet used by Tubbs et al. (9) is highly inflammatory and rapidly alters muscle integrity compared with the HFD used in our study (45,46). In addition, a method adopted by Tubbs et al. (9) for quantifying the MAM amount by isolation of MAM fraction is not a robust method when comparing healthy and unhealthy groups. High-fat, high-sucrose diet skeletal muscle tissue induces mitochondrial damage (47); therefore, there is a high chance of losing the MAM population associated with the damaged mitochondria during the subcellular fractionation process. Therefore, quantifying the protein concentration from isolated MAM homogenates to determine the MAM amount might give inaccurate information. We also cannot rule out that the differences in species (human vs. mouse), cell culture conditions, and time periods chosen for analysis may result in different findings, as MAM is highly dynamic in response to environmental factors and cellular status (40). Furthermore, our findings agree well with the finding that patients with nonalcoholic steatohepatitis have increased expression of IP3R1, and the amount of MAM correlated with the degree of steatosis in human liver biopsies (48). Thus, we postulate that the discrepancy between these two studies may be explained primarily by difference in diets but also by methodology and experimental conditions.

JNK is known to mediate IR under conditions of mitochondrial dysfunction and ER stress (49). Previously, JNK1 deficiency has been shown to prevent diet-induced IR in skeletal muscle (50). We observed that deficiency of PDK4 and other MAM components suppressed JNK1 activation to ameliorate IR. Consistent with these findings, we recently reported that cisplatin-induced JNK activation is suppressed by pharmacological inhibition or genetic ablation of PDK4 (16). We also found that artificial enhancement of ER–mitochondria coupling using a synthetic ER–mitochondria linker triggered JNK1 activation and reduced insulin-induced AKT activation in myotubes. These detrimental effects of linker overexpression were reversed by pharmacological inhibition of JNK, suggesting that linker-mediated IR is dependent on JNK activation. This is in line with a previous study showing that artificial enrichment of ER–mitochondrial contacts instigates obesity-induced hepatic IR via a JNK-dependent mechanism (4).

Overall, we conclude that PDK4 deficiency leads to destabilization of the IP3R1-GRP75-VDAC1 complex, which subsequently leads to the suppression of JNK activation and protects from skeletal muscle IR in the context of obesity. Our data provide important evidence that MAM is associated with skeletal muscle IR and identifies PDK4 as a novel modulator of MAM integrity. Our study strengthens the notion that modulating MAM formation could be a promising strategy for the treatment of obesity-related metabolic diseases.

Funding. This work was supported by National Research Foundation of Korea grants funded by the Korean government (Ministry of Science, ICT and Future Planning) (NRF-2016M3A9B6902872, NRF-2017R1A2B3006406, NRF-2016R1E1A2020567, and NRF-2017R1E1A2A02023467), a grant of the Korea Health Technology R&D Project through the Korea Health Industry Development Institute, funded by the Ministry of Health & Welfare, Republic of Korea (HI16C1501), a grant funded by the Korea Basic Science Institute (T38210), VA Merit Award 1I01CX000361, National Institutes of Health grants U01-AA-021840, R01-DK-107682, R01-AA-025208, and U.S. Department of Defense grant W81XWH-12-1-0497.

Duality of Interest. No potential conflicts of interest relevant to this article were reported.

Author Contributions. T.T. performed experiments and analyzed and interpreted data. T.T., J.L., and I.-K.L. designed experiments, discussed data, and wrote the manuscript. C.-M.H., J.-S.P., H.-J.K., Y.H.H., and K.-S.P. contributed to experiments and data collection. J.-H.J., S.L., Y.H.H., T.-H.K., K.-G.P., R.A.H., H.-W.R., and K.-S.P. provided reagents and materials and discussed data. T.T., D.C., Y.-K.C., S.L., R.A.H., and I.-K.L. edited and revised the manuscript. I.-K.L. supervised the work. I.-K.L. is the guarantor of this work and, as such, had full access to all of the data in the study and takes responsibility for the integrity of the data and the accuracy of the data analysis.

References

1. Arruda AP, Hotamisligil GS. Calcium homeostasis and organelle function in the pathogenesis of obesity and diabetes. Cell Metab 2015;22:381–397

2. Szabadkai G, Bianchi K, Várnai P, et al. Chaperone-mediated coupling of endoplasmic reticulum and mitochondrial Ca2+ channels. J Cell Biol 2006;175:901–911

3. Tubbs E, Theurey P, Vial G, et al. Mitochondria-associated endoplasmic reticulum membrane (MAM) integrity is required for insulin signaling and is implicated in hepatic insulin resistance. Diabetes 2014;63:3279–3294

4. Arruda AP, Pers BM, Parlakgül G, Güney E, Inouye K, Hotamisligil GS. Chronic enrichment of hepatic endoplasmic reticulum-mitochondria contact leads to mitochondrial dysfunction in obesity. Nat Med 2014;20:1427–1435

5. Rieusset J, Fauconnier J, Paillard M, et al. Disruption of calcium transfer from ER to mitochondria links alterations of mitochondria-associated ER membrane integrity to hepatic insulin resistance. Diabetologia 2016;59:614–623
6. Bouzakri K, Koistinen HA, Zierath JR. Molecular mechanisms of skeletal muscle insulin resistance in type 2 diabetes. Curr Diabetes Rev 2005;1:167–174
7. Gonzalez-Franquesa A, Patti ME. Insulin resistance and mitochondrial dysfunction. Adv Exp Med Biol 2017;982:465–520
8. Salvadó L, Palomer X, Barroso E, Vázquez-Carrera M. Targeting endoplasmic reticulum stress in insulin resistance. Trends Endocrinol Metab 2015;26:438–448
9. Tubbs E, Chanon S, Robert M, et al. Disruption of mitochondria-associated endoplasmic reticulum membrane (MAM) integrity contributes to muscle insulin resistance in mice and humans. *Diabetes* 2018;67:636–650
10. Zhang S, Hulver MW, McMillan RP, Cline MA, Gilbert ER. The pivotal role of pyruvate dehydrogenase kinases in metabolic flexibility. Nutr Metab (Lond) 2014;11:10
11. Bowker-Kinley MM, Davis WI, Wu P, Harris RA, Popov KM. Evidence for existence of tissue-specific regulation of the mammalian pyruvate dehydrogenase complex. Biochem J 1998;329:191–196
12. McAinch AJ, Cornall LM, Watts R, Hryciw DH, O'Brien PE, Cameron-Smith D. Increased pyruvate dehydrogenase kinase expression in cultured myotubes from obese and diabetic individuals. Eur J Nutr 2015;54:1033–1043
13. Jeoung NH, Harris RA. Pyruvate dehydrogenase kinase-4 deficiency lowers blood glucose and improves glucose tolerance in diet-induced obese mice. Am J Physiol Endocrinol Metab 2008;295:E46–E54
14. Hwang B, Jeoung NH, Harris RA. Pyruvate dehydrogenase kinase isoenzyme 4 (PDHK4) deficiency attenuates the long-term negative effects of a high-saturated fat diet. Biochem J 2009;423:243–252
15. Lee SJ, Jeong JY, Oh CJ, et al. Pyruvate dehydrogenase kinase 4 promotes vascular calcification via SMAD1/5/8 phosphorylation [published correction appears in Sci Rep 2006;6:18552]. Sci Rep 2015;5:16577
16. Oh CJ, Ha CM, Choi YK, et al. Pyruvate dehydrogenase kinase 4 deficiency attenuates cisplatin-induced acute kidney injury. Kidney Int 2017;91:880–895
17. Liu Z, Du X, Deng J, et al. The interactions between mitochondria and sarcoplasmic reticulum and the proteome characterization of mitochondrion-associated membrane from rabbit skeletal muscle. Proteomics 2015;15:2701–2704
18. Pasut A, Jones AE, Rudnicki MA. Isolation and culture of individual myofibers and their satellite cells from adult skeletal muscle. J Vis Exp 2013;73:e50074
19. Wynn RM, Kato M, Chuang JL, Tso SC, Li J, Chuang DT. Pyruvate dehydrogenase kinase-4 structures reveal a metastable open conformation fostering robust core-free basal activity. J Biol Chem 2008;283:25305–25315
20. Csordás G, Renken C, Várnai P, et al. Structural and functional features and significance of the physical linkage between ER and mitochondria. J Cell Biol 2006;174:915–921
21. Wieckowski MR, Giorgi C, Lebiedzinska M, Duszynski J, Pinton P. Isolation of mitochondria-associated membranes and mitochondria from animal tissues and cells. Nat Protoc 2009;4:1582–1590
22. Frezza C, Cipolat S, Scorrano L. Organelle isolation: functional mitochondria from mouse liver, muscle and cultured fibroblasts. Nat Protoc 2007;2:287–295
23. Kuznetsov AV, Kehrer I, Kozlov AV, et al. Mitochondrial ROS production under cellular stress: comparison of different detection methods. Anal Bioanal Chem 2011;400:2383–2390
24. Sakellariou GK, Pearson T, Lightfoot AP, et al. Mitochondrial ROS regulate oxidative damage and mitophagy but not age-related muscle fiber atrophy. Sci Rep 2016;6:33944
25. Yazıcı D, Sezer H. Insulin resistance, obesity and lipotoxicity. Adv Exp Med Biol 2017;960:277–304
26. Jeong JY, Jeoung NH, Park KG, Lee IK. Transcriptional regulation of pyruvate dehydrogenase kinase. Diabetes Metab J 2012;36:328–335
27. Giacomello M, Pellegrini L. The coming of age of the mitochondria-ER contact: a matter of thickness. Cell Death Differ 2016;23:1417–1427
28. Egnatchik RA, Leamy AK, Jacobson DA, Shiota M, Young JD. ER calcium release promotes mitochondrial dysfunction and hepatic cell lipotoxicity in response to palmitate overload. Mol Metab 2014;3:544–553
29. Palmer AE, Tsien RY. Measuring calcium signaling using genetically targetable fluorescent indicators. Nat Protoc 2006;1:1057–1065
30. Henning RH, Duin M, van Popta JP, Nelemans A, den Hertog A. Different mechanisms of Ca2(+)-handling following nicotinic acetylcholine receptor stimulation, P2U-purinoceptor stimulation and K(+)-induced depolarization in C2C12 myotubes. Br J Pharmacol 1996;117:1785–1791
31. Palmer AE, Jin C, Reed JC, Tsien RY. Bcl-2-mediated alterations in endoplasmic reticulum Ca2+ analyzed with an improved genetically encoded fluorescent sensor. Proc Natl Acad Sci U S A 2004;101:17404–17409
32. Ly LD, Xu S, Choi SK, et al. Oxidative stress and calcium dysregulation by palmitate in type 2 diabetes. Exp Mol Med 2017;49:e291
33. Jheng HF, Tsai PJ, Guo SM, et al. Mitochondrial fission contributes to mitochondrial dysfunction and insulin resistance in skeletal muscle. Mol Cell Biol 2012;32:309–319
34. Porter C, Wall BT. Skeletal muscle mitochondrial function: is it quality or quantity that makes the difference in insulin resistance? J Physiol 2012;590:5935–5936
35. Zhang D, Armstrong JS. Bax and the mitochondrial permeability transition cooperate in the release of cytochrome c during endoplasmic reticulum-stress-induced apoptosis. Cell Death Differ 2007;14:703–715
36. Solinas G, Becattini B. JNK at the crossroad of obesity, insulin resistance, and cell stress response. Mol Metab 2016;6:174–184
37. van Vliet AR, Verfaillie T, Agostinis P. New functions of mitochondria associated membranes in cellular signaling. Biochim Biophys Acta 2014;1843:2253–2262
38. Yi M, Weaver D, Eisner V, et al. Switch from ER-mitochondrial to SR-mitochondrial calcium coupling during muscle differentiation. Cell Calcium 2012;52:355–365
39. Tjondrokoesoemo A, Li N, Lin PH, et al. Type 1 inositol (1,4,5)-trisphosphate receptor activates ryanodine receptor 1 to mediate calcium spark signaling in adult mammalian skeletal muscle. J Biol Chem 2013;288:2103–2109
40. Eisner V, Csordás G, Hajnóczky G. Interactions between sarco-endoplasmic reticulum and mitochondria in cardiac and skeletal muscle - pivotal roles in Ca^{2+} and reactive oxygen species signaling. J Cell Sci 2013;126:2965–2978
41. Tarasov AI, Griffiths EJ, Rutter GA. Regulation of ATP production by mitochondrial Ca(2+). Cell Calcium 2012;52:28–35
42. Bravo R, Vicencio JM, Parra V, et al. Increased ER-mitochondrial coupling promotes mitochondrial respiration and bioenergetics during early phases of ER stress. J Cell Sci 2011;124:2143–2152
43. Samovski D, Sun J, Pietka T, et al. Regulation of AMPK activation by CD36 links fatty acid uptake to β-oxidation. Diabetes 2015;64:353–359
44. Salvadó L, Coll T, Gómez-Foix AM, et al. Oleate prevents saturated-fatty-acid-induced ER stress, inflammation and insulin resistance in skeletal muscle cells through an AMPK-dependent mechanism. Diabetologia 2013;56:1372–1382
45. Ishimoto T, Lanaspa MA, Rivard CJ, et al. High-fat and high-sucrose (western) diet induces steatohepatitis that is dependent on fructokinase. Hepatology 2013;58:1632–1643
46. Collins KH, Paul HA, Hart DA, et al. A high-fat high-sucrose diet rapidly alters muscle integrity, inflammation and gut microbiota in male rats. Sci Rep 2016;6:37278
47. Bonnard C, Durand A, Peyrol S, et al. Mitochondrial dysfunction results from oxidative stress in the skeletal muscle of diet-induced insulin-resistant mice. J Clin Invest 2008;118:789–800
48. Feriod CN, Oliveira AG, Guerra MT, et al. Hepatic inositol 1,4,5 trisphosphate receptor type 1 mediates fatty liver. Hepatol Commun 2017;1:23–35
49. Li H, Yu X. Emerging role of JNK in insulin resistance. Curr Diabetes Rev 2013;9:422–428
50. Sabio G, Kennedy NJ, Cavanagh-Kyros J, et al. Role of muscle c-Jun NH2-terminal kinase 1 in obesity-induced insulin resistance. Mol Cell Biol 2010;30:106–115